Journal of Sound and Vibration 425 (2018) 324–343

Contents lists available at ScienceDirect

Journal of Sound and Vibration

journal homepage: www.elsevier.com/locate/jsvi

On the leading edge noise and aerodynamics of thin aerofoil subjected to the straight and curved serrations

Auris Juknevicius, Tze Pei Chong*

Department of Mechanical and Aerospace Engineering, Brunel University London, Uxbridge, UB8 3PH, United Kingdom

ARTICLE INFO

Article history:
Received 25 June 2017
Received in revised form 9 February 2018
Accepted 19 February 2018

Keywords:
Serrated leading edge
Broadband noise reduction
Boundary layer separation

ABSTRACT

This paper presents the results of an experimental study into the effect of add-on type leading edge serrations on the aeroacoustic and aerodynamic performances of a symmetrical NACA0008 aerofoil. The aeroacoustic part of this paper studies the reduction of interaction broadband noise in the presence of elevated freestream turbulence by employing serrated leading edges. For non-dimensional frequencies $f' < 1$, the resulting sound pressure level reduction (ΔSPL) was found to be a linear function of f' and the ΔSPL depends only on the serration amplitude, serration wavelength and freestream velocity. Leading edge with a large serration amplitude was found to be very effective in the reduction of broadband noise where up to ΔSPL ≈ 8 dB is achievable. It is generally more beneficial to choose a leading edge with a smaller serration wavelength, although the most effective configuration actually combines the largest serration amplitude and the largest serration wavelength. Interestingly, for a curved-serration, the most optimised configuration (with small serration wavelength, large serration amplitude, small inclination angle and large curvature radius) was found to outperform its straight-serration counterpart by a further 5 dB reduction of broadband noise at the same frequency. Concerning the aerodynamic part of the study, to effectively suppress boundary layer stall without incurring severe drag penalties for low freestream turbulence intensity, the most effective leading edge serration should possess a large serration wavelength and small serration amplitude. Hence, the serration geometry that works very well for a low noise aerofoil is usually inferior in the aerodynamic performance, and vice versa. The best compromise for the serration geometry that can still harness good performances in both the aeroacoustic and aerodynamic should possess the largest serration amplitude and the largest serration wavelength. This paper demonstrates that, when optimised properly, the add-on type leading edge serration can be very effective in both the reduction of the interaction broadband noise, and the suppression of the boundary layer separation at high angle of attack.

1. Introduction

It has been shown that noise generated by many industrial operations produces considerable negative impact on the environment, which has become an increasingly sensitive topic. In particular, the civil aviation industry is a substantial

* Corresponding author.
E-mail address: t.p.chong@brunel.ac.uk (T.P. Chong).

https://doi.org/10.1016/j.jsv.2018.02.038

contributor to the noise pollution levels on a global scale. As a result, it is receiving significant attention in terms of its impact on the communities surrounding the large airports. The forecast of the annual growth of air passengers calls for regulations to be implemented by the airports or local authorities. The ACARE Flightpath 2050 initiative aims to achieve a 65% reduction in commercial aviation noise emissions by 2050, relative to the level in the year 2000. Historically, aircraft and turbomachinery manufacturers always strive to improve the aerodynamics and manoeuvrability of their aircraft. More recently, the focus has shifted to the development of advanced and efficient aero-engines that produce smaller carbon footprints and noise radiation levels. To a large extent, the jet noise has been reduced considerably due to the introduction of large bypass ratio aero-engines. As a result, other aircraft noise sources (e.g. airframe noise, fan noise and combustion noise) become increasingly important.

The wind turbine industry is another major sector that actively seeks to develop the latest aerofoil noise reduction technology for their turbine blades. This is especially important as the drive for sustainable low-carbon energy sources has led to a significant expansion in the number of wind farms that expose surrounding communities to significant noise levels. To mitigate the noise pollution effects, wind farms are usually constructed in low populated areas.

Whilst trailing edge self-noise from aerofoil blades is traditionally a significant noise source, the importance of leading edge-turbulence interaction noise is also well established. Previously, it has been shown that leading edge noise is usually related to large-scale turbulence structures in the freestream. These turbulence structures interact with the leading edge of an aerofoil before being stretched around it. During the stretching process, large pressure fluctuations can be induced on the suction and pressure surfaces of the aerofoil. Significant levels of broadband noise radiation are produced by the amplified unsteady lift [1]. To reduce the leading edge noise, one of the most effective methods is to apply an owl-wing inspired serrated pattern at the leading edge. Some studies performed on the owl's silent flight (mainly through measurements of mid-flight noise emission) have led to postulation that these serrations could be partially responsible for the unique in-flight noise reduction capability of an owl. The following literature review will briefly summarise the use of serration technology for aerofoil leading edge noise reduction.

In the 1970's, the effect of the leading edge serration originally tested by Soderman et al. [2] was further investigated by Hersh and Hayden [3] for its ability to reduce aerofoil tonal noise from helicopter blades. They showed that leading edge serrations can achieve a noise reduction between 4 and 8 dB. Recently, there is renewed interest to apply leading edge serration to achieve aerofoil turbulence-leading edge interaction noise reduction. In a joint experimental-numerical effort by Clair et al. [4], the serrated leading edge of an NACA 65-(12)10 aerofoil is found to achieve a broadband noise reduction between 3 and 4 dB. Narayanan et al. [5] assess the effects of a serrated leading edge on the turbulence-leading edge interaction noise for a flat plate, as well as a NACA 65-(12)10 aerofoil. A near isotropic turbulence was produced using a grid inside the nozzle. They demonstrated a significant broadband noise reduction of 9 dB for a flat plate and 7 dB for an aerofoil configuration, respectively, using the largest serration amplitude. They suggested that the level of broadband noise reduction is a strong function of the serration amplitude h, and is less sensitive to the serration wavelength λ. An inviscid numerical study by Kim et al. [6] exhibited a de-correlation of the surface pressure fluctuation and the far field noise on a serrated leading edge. In particular, the noise source at the mid-region of the oblique edge becomes ineffective across the mid to high frequency range. Another noise reduction mechanism is attributed to the phase interference and destruction effect between the serration peak and the mid-region of the oblique edge. Chaitanya et al. [7] reports that the optimum noise reduction performance should correspond to the case where adjacent noise sources at the sawtooth troughs are incoherent. They have identified that the optimum serration wavelength λ should be roughly equal to four times the incoming turbulence integral length. Apart from the h and λ, the serrated leading edge is also found to be sensitive to other influencing parameters such as the Reynolds number, turbulence intensity and angle of attack. These interdependencies of factors were studied empirically by Biedermann et al. [8] to model the serrated leading edge noise.

So far, the leading edge device for the reduction of interaction broadband noise is almost exclusively formed by the cut-in approach, i.e. the serration pattern is cut into the main body of the aerofoil. The design and manufacturing complexities of the cut-in serration are the obvious disadvantages. The next technological step to produce leading edge serration is to simplify the design and manufacturing processes. In contrast to the cut-in approach, leading edge serrations can also be achieved as an add-on (just like the trailing edge serration). The anti-stall capability of aerofoil with an add-on type leading edge serration has already been reported by Ito [9]. The first objective of this paper is to address whether an add-on serrated leading edge can produce a similar level of interaction broadband noise reduction typically achieved by those of the cut-in type.

As observed by the ornithologists, the leading edge of an owl's wing exhibits a comb-like “curved” serration. Such curvature adds to two further geometrical parameters such as the inclination angle and the curvature radius. Furthermore, the curved-flow path within the sawtooth gap will produce an effective serration amplitude h', which is normally longer than the h counterpart for an otherwise straight serration. The second objective of this paper, therefore, is to exploit this unique morphology of the owl wing for the leading edge serration on an aerofoil. As pointed out by Kim et al. [6], the remaining contributor to the interaction noise radiation for a serrated leading edge is related to the flow dynamics at the sawtooth trough region. Because each consecutive sawtooth tip of a curved leading edge serration exhibits a spanwise offset relative to the sawtooth trough, the incoming turbulence structures could perhaps be shielded by the inclined sawtooth tip. This has the potential to reduce the level of turbulence interaction at the trough, which might lead to a further reduction of the broadband interaction noise level.

2. Experimental setup

2.1. Wind tunnel facilities, instrumentation and grid-generated turbulence

Free field measurements of the aerofoil noise were conducted in the aeroacoustic open jet wind tunnel at Brunel University London, which is situated in a 4 m × 5 m x 3.4 m anechoic chamber. As shown in Fig. 1, the nozzle exit is a rectangle with a height of 0.1 m and a width of 0.3 m. This wind tunnel can achieve freestream turbulence intensity of between 0.1 and 0.2% and maximum jet velocity of about 80 ms^{-1}. The background noise of the wind tunnel facility is well below the self noise of the quietest aerofoil across the whole range of velocities [10]. The range of jet speeds under investigation here was $20 \leq U_{\infty} \leq 60\ ms^{-1}$, which correspond to chord-based Reynolds numbers of $2 \times 10^5 \leq Re \leq 6 \times 10^5$, respectively. The aerofoil was held by side plates and attached smoothly against the nozzle lips.

Fig. 1 also shows that a single condenser microphone at a polar angle of about 90° and a distance of 1.0 m from the aerofoil leading edge at mid span was used for the far field noise measurements. Noise data was acquired at a sampling frequency of 44 kHz for 15 s by a 16-bit Analogue-Digital card from National Instrument. The data was then windowed and the Power Spectral Density (PSD) of 1 Hz bandwidth and a frequency resolution of 43 Hz was subsequently computed using a 1024-point Fast Fourier Transform.

To generate large scale turbulence structures, and obtain an elevated level of turbulence intensity in the freestream, a bi-planar orthogonal square grid, measuring a total width (W_{Grid}) of 378 mm and a total height (H_{Grid}) of 270 mm, was placed inside the nozzle. The mesh length of each individual grid element (M) is 75 mm and the grid diameter (d) is 15 mm. Hot-wire measurement of the freestream turbulence intensity and eddy integral length scale at location near the aerofoil leading edge (but without the presence of the aerofoil) are 3.7% and 6.5 mm, respectively. In our previous publications [8,11], the above bi-planar grid has been demonstrated to be able to achieve isotropic turbulence of reasonably quality with a good agreement between the normalised turbulence energy spectra of the fluctuation velocity measured by the hot-wire and the Von Karman and Liepmann's one-dimensional turbulence model.

It should be noted that the presence of an elevated turbulence intensity in the freestream will trigger a bypass transition leading to the boundary layer becoming turbulent relatively close to the aerofoil's leading edge. Essentially, the transition point is dictated by the elevated freestream turbulence intensity, instead of the streamwise vortices generated by the serrated leading edge. As a result, the radiation of the turbulent boundary layer-trailing edge noise is not too sensitive to the different choices of the add-on serrated leading edges. Fig. 2 shows the Sound Pressure Level (SPL) spectra produced by a baseline aerofoil ($\lambda 0h0$ – the basis of the naming will be discussed in Section 2.2) for two cases: one has a clean surface while the other contains a boundary layer tripping element on both the upper and lower surfaces (placed at 20% of the chord from the leading edge). The fact that the noise spectra are almost identical for both cases supports the argument above. The same trend in noise spectra can also be observed when the leading edge is replaced by a serrated type. Also shown in Fig. 2 are the SPL spectra produced by the clean and tripped cases for an aerofoil with the $\lambda 20h30$ serrated leading edge (the basis of the naming will also be discussed in Section 2.2). Both spectra are essentially the same across the whole frequency range. Although not included here for brevity, the same outcome can also be produced by employing other types of serrated leading edges across the whole velocity range investigated here. Therefore, any difference in characteristics for the noise spectra presented throughout the current paper is due to the leading edge geometry only. It is necessary to emphasise that no boundary layer trip tape was implemented on the aerofoil in the experiments (except for the verification test in Fig. 2).

Aerodynamic force measurements were made in a conventional closed-working section wind tunnel, which has a test section of 0.5 m × 0.5 m. The maximum velocity in the test section is about 38 ms^{-1}, with a typical freestream turbulence intensity at about 0.2–0.3%. The aerofoil model was mounted horizontally across almost the entire width of the test section

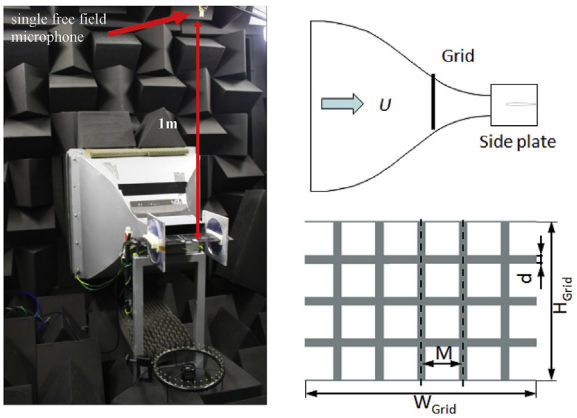

Fig. 1. A typical set up for the aerofoil noise experiments at the Brunel aeroacoustic wind tunnel for the turbulence–leading edge interaction noise. The placement of the turbulence bi-planar grid with relative to the nozzle is shown.

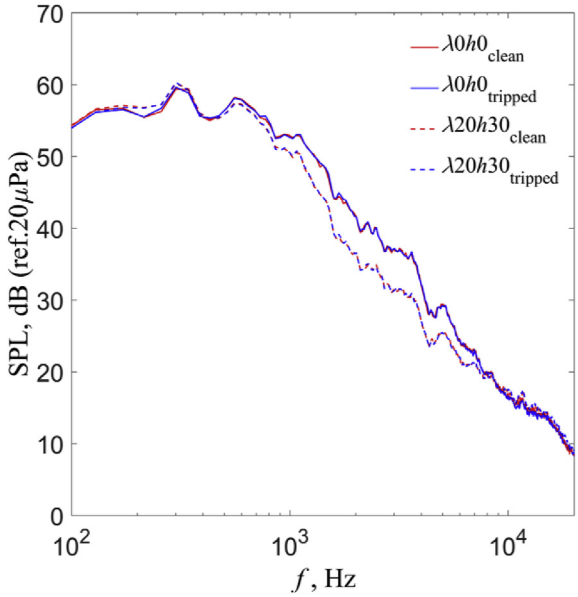

Fig. 2. Comparison of the SPL spectra (dB, ref 20 μPa) produced by the baseline ($\lambda 0h0$) and a serrated ($\lambda 20h30$) leading edges with both clean and tripped surfaces on the aerofoil body at $U_\infty = 50\,\mathrm{ms}^{-1}$.

(1 mm gap on each side of the wind tunnel side window). A 3-component strain gauge force balance was used to measure the uncorrected lift and drag forces produced by the baseline and serrated aerofoil. The presence of solid walls in the wind tunnel will prevent a normal curvature of the flow streamline especially when the aerofoil is subjected to a non-zero angle of attack. This represents the solid-blockage effect that can lead to inaccuracy in the lift and drag measurements. Another source of inaccuracy is related to the wake-blockage effect. This phenomenon can result in a higher freestream velocity at the downstream of the aerofoil than that at the upstream. This will induce a streamwise pressure gradient, thereby changing the static pressure distribution on the aerofoil surfaces. In the current study, standard correction procedures [12] for the solid-blockage and wake-blockage effects have been applied to the raw data of the lift and drag forces.

The effects of the angle of attack on the leading edge noise and aerodynamic forces have been investigated in the open jet wind tunnel and aerodynamic wind tunnel, respectively. The symbol α refers to the "geometrical" angle of attack defined in the open jet wind tunnel for the aeroacoustic tests. It should be mentioned that α is not the true angle of attack because the pressure loading on the aerofoil will be affected by the open jet deflection. On the other hand, the "effective" angle of attack $\alpha_{(\mathrm{effective})}$, which is the true angle of attack, is defined in the aerodynamic closed-section aerodynamic wind tunnel. Note that for each leading edge device, three raw datasets for the lift and drag forces were acquired. The mean values of the raw datasets represent the averaged aerodynamic forces.

2.2. Design of the aerofoil and the leading edge serrations

Thin aerofoil is commonly adopted in the OGV (Outlet Guided Vanes) configuration, or in a compressor cascade. It also features a large curvature at the leading edge. This means that, in comparison to a thicker aerofoil, the incoming turbulence structures to a thin aerofoil will be deprived of the mechanism of acceleration around the leading edge. As a result, high levels of broadband noise will be radiated due to the significant turbulence-solid structure interaction. The NACA0008, which has a maximum thickness equivalent to 8% of the chord, was selected in this study. The chord length of the aerofoil, C, is 0.15 m. The maximum aerofoil thickness is 12 mm and the span of the aerofoil is $b = 0.498$ m. Note that during the noise measurement, only $b = 0.3$ m of the aerofoil was submerged in the jet flow, where the excess parts were extended beyond the side plates of the open jet nozzle. The full width of the aerofoil was utilised during the measurement of the aerodynamic forces at the aerodynamic wind tunnel with a closed-working section.

The aerofoil has been designed so that the first 25 mm of the body (starting from the leading edge) is detachable. Note that one of the detachable leading edges provides a straight leading edge (i.e. without slot at the nose) to serve as the "clean" baseline aerofoil shape ($\lambda 0h0$). Another detachable leading edge incorporates a slot with thickness = 0.8 mm and inner-length of 17 mm that runs along the chord line of the aerofoil from the leading edge. The slot allows various serration inserts to be slotted in and interchanged with other inserts easily. The flat plate serration inserts were laser-cut precisely using cardboard sheets of about 0.8 mm thickness. This material can achieve sufficient accuracy in terms of the serration dimensions. Despite the relatively thin structure, the serration inserts can adequately provide the required stiffness to avoid fluttering during experiments.

The first type of serrations is the regular, straight sawtooth serrations shown in Fig. 3a. To gain a better understanding of the effect of serration geometry on the aeroacoustic performance, a wide range of serration geometries was designed. There are two main and independent design parameters: the serration wavelength λ and serration amplitude h. The serration angle $\phi = \tan^{-1}(\lambda/2h)$, depicted in the figure, is a function of both λ and h. The serration dimensions are $\lambda = 2.5, 5, 10, 15, 20$ mm; and $h = 5, 10, 15, 20, 30$ mm, giving a total of 25 straight-sawtooth serrated leading edge variations. Note that the naming of each serrated leading edge, including the baseline case, is in accordance to the values of their serration wavelength λ, and serration amplitude h. For example, the "clean", baseline leading edge mentioned in the previous paragraph, which does not contain any serration wavelength and serration amplitude, is therefore named as $\lambda 0h0$. Likewise, the serrated leading edge that has a serration wavelength of 2.5 mm and serration amplitude of 30 mm is named as $\lambda 2.5h30$. In Section 2.3, noise results produced

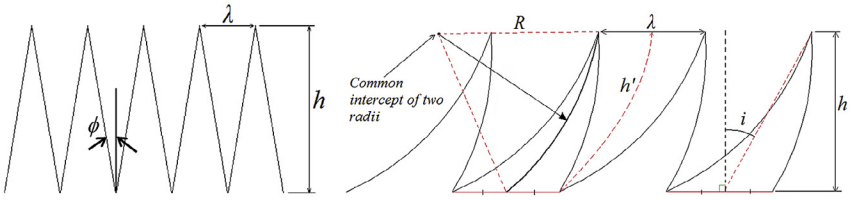

Fig. 3. Geometrical parameters for a (a) straight-serration, and (b) curved-serration.

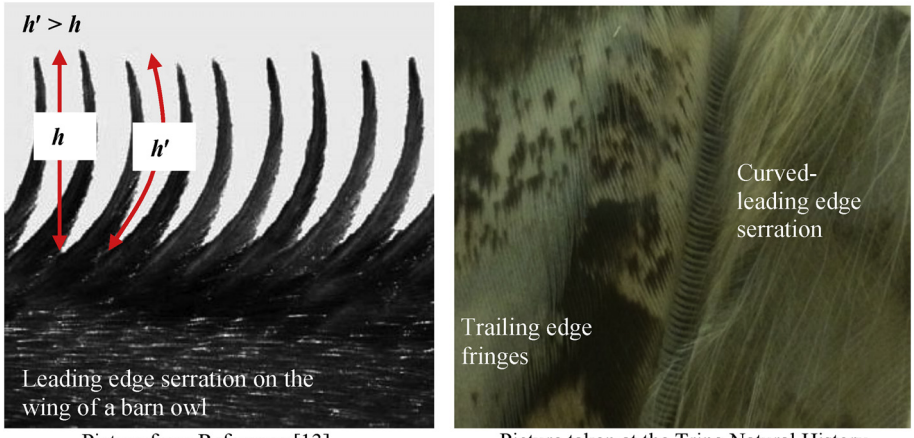

Fig. 4. (a) Examples of curved-leading edge serration on owls, and (b) curved-serrated leading edge attached to the NACA0008 model.

by a straight, unserrated flat plate add-on are also presented. This baseline configuration with flat plate add-on is identified by $\lambda 0h$XX, where XX is the longitudinal length of the add-on.

Fig. 4a shows two examples of leading edge serrations on owl wings, including one from Bachmann et al. [13], to demonstrate the unique serration in curvature. This feature is replicated in the current NACA0008 aerofoil (see e.g. Fig. 4b). Note that these curved-serrations were manufactured using a similar technique as for the straight serration. As shown in Fig. 3b, the curved serration designs are based on five main geometric parameters: the serration wavelength λ, serration amplitude (straight) h, serration amplitude (curved) h', inclination angle i and curvature radius R (where a large serration curvature is characterised by a small radius R). In the current study, the curved-serrations are designed to have two inclination angles $i = 15^\circ$ and 30°, and two curvature radii $R = 50$ mm and 100 mm. These provide a total of four types of curved serration for each combination of λ and h, which cover an adequate number of geometry parameter variations. As a result, the curvature effect on the aeroacoustic performances can be reasonably generalised. It is also worth pointing out that the values for $i = 15^\circ$ and $R = 50$ mm provide a serration pattern that is visually quite similar to those found in the owl's wings. The basis for the naming of the curved-serration follows the same logic. For example, the combination $\lambda = 2.5$ mm, $h = 30$ mm, $i = 15^\circ$ and $R = 50$ mm, is identified by $\lambda 2.5h30(i15^\circ R50)$. A straight serration with the same combination of λ and h will be identified by either $\lambda 2.5h30$(straight), or simply be $\lambda 2.5h30$.

2.3. Definition of the baseline leading edge

It is important to correctly define the baseline configuration of the leading edge to allow unbiased comparisons between the baseline results and results obtained employing the various serrated leading edges. There are two candidates for the baseline. The first candidate is the $\lambda 0h0$ type without flat plate insert at the leading edge. The second candidate is the $\lambda 0h$XX type where an unserrated, straight flat plate insert profile is attached to the leading edge. For the second choice its longitudinal length needs to be half of the corresponding add-on serrated leading edge in order to match their respective wetted areas. For example, a serrated leading edge with $h = 30$ mm will be compared against a straight, add-on baseline leading edge of $h = 15$ mm (i.e. $\lambda 2.5h30$ vs. $\lambda 0h15$).

Fig. 5a shows the SPL spectra for the $\lambda 0h0$, $\lambda 20h5$ and $\lambda 0h2.5$ cases at $U_\infty = 50\ \mathrm{ms}^{-1}$ (corresponding to $Re = 5 \times 10^5$). From the figure, the SPL produced by the serrated $\lambda 20h5$ case is very similar to the $\lambda 0h0$ baseline case for $f < 4$ kHz. Above this frequency, however, the SPL of $\lambda 20h5$ is consistently higher than that of $\lambda 0h0$. This means that compared to the baseline case, the serrated $\lambda 20h5$ case not only fails to reduce the broadband noise, but also increases the noise level by up to 8 dB at high frequencies. However, when comparing the serrated $\lambda 20h5$ case to the flat plate baseline $\lambda 0h2.5$ case, broadband noise reduction is achieved across a large range of frequencies for $f > 2$ kHz.

A similar trend can also be observed when using the $\lambda 2.5h30$ serrated leading edge (see Fig. 5b). It will be shown later that $\lambda 2.5h30$ is one of the best configurations for achieving broadband noise reduction. While it outperforms the $\lambda 0h0$ baseline for

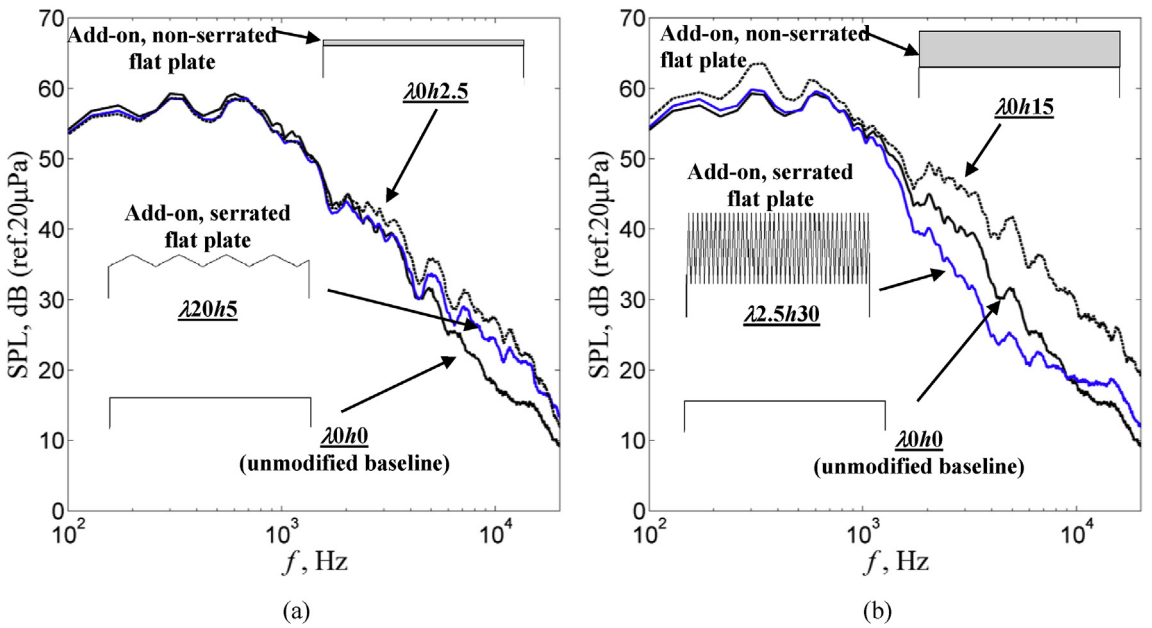

Fig. 5. Comparison of the SPL spectra (dB, ref 20 μPa) produced by the unmodified baseline ($\lambda 0h0$), against the (a) baseline with add-on flat plate ($\lambda 0h2.5$) and add-on serrated leading edges ($\lambda 20h5$), and the (b) baseline with add-on flat plate ($\lambda 0h15$) and add-on serrated leading edges ($\lambda 2.5h30$). $U_\infty = 50\ \mathrm{ms}^{-1}$.

$1 < f < 9$ kHz, the level of noise reduction is even more impressive over almost the entire frequency range when comparing it to the $\lambda 0h15$ baseline.

By adding an unserrated, straight flat-plate insert to the aerofoil leading edge, the noise level will generally increase. The noise level is also found to increase when the longitudinal length of the flat plate is increased. It is clear that the above insert cannot be a meaningful baseline case to be compared against other add-on serrated leading edges because the level of broadband noise reduction will be exaggerated. After all, the industrial fan blades are unlikely to contain an unserrated flat plate at their leading edges in the first place. Therefore, the unmodified baseline case $\lambda 0h0$ is selected for noise comparison throughout this paper.

3. General aeroacoustic characteristics of the straight-serrated leading edges

This section will present the experimental results pertaining to the broadband noise reduction by the straight-serrated leading edges. The results presented earlier in Fig. 5 already indicated the sensitivity of the level of broadband noise reduction to λ and h. Here, the level of noise reduction is denoted as ΔSPL, which is defined as $\mathrm{SPL}(\lambda 0h0) - \mathrm{SPL}(\lambda xhy)$, where $x \in 2.5, 5, 10, 15, 20$ mm, and $y \in 5, 10, 15, 20, 30$ mm. A positive value of ΔSPL represents a reduction in the noise level by the serrated leading edge, and a negative value represents a noise increase. A large amount of data was available for the ΔSPL spectra, which cover the 25 types of straight-serrated leading edges for $2 \times 10^5 \leq Re \leq 6 \times 10^5$. After analysing all datasets, the ΔSPL for the leading edge broadband noise can be fitted reasonably well by an empirical linear function at the frequency region when the leading edge interaction noise is significant:

$$\Delta\mathrm{SPL} = Gf' + \kappa \mathrm{Re}^{-0.12}, \quad \text{where} \quad \begin{pmatrix} G = 12, \ [\mathrm{dB}] \\ f' = \dfrac{fh}{U_\infty}\left(\dfrac{\lambda}{C}\right)^{0.2} \\ \kappa = -9.7, \ [\mathrm{dB}] \end{pmatrix} \tag{1}$$

Some examples are illustrated in Fig. 6a and b for $Re = 3 \times 10^5$ and 6×10^5, respectively. The use of a non-dimensional frequency f', which is scaled by h, λ, U_∞ and C is found to provide a good collapse of the curves amongst the serrated leading edges at $f' < 1$. Note that Eq. (1) is characterised by the gradient $G = 12$, which represents the upper-limit of ΔSPL at $f' < 1$ that is achievable by a standard, straight-serrated leading edge with any combinations of λ and h. It should be noted that this function, however, is not quite universal because the effects of freestream turbulence intensity, turbulence length scale and angle of attack have not been investigated. Nevertheless, the results demonstrate that the serration amplitude, h, is more

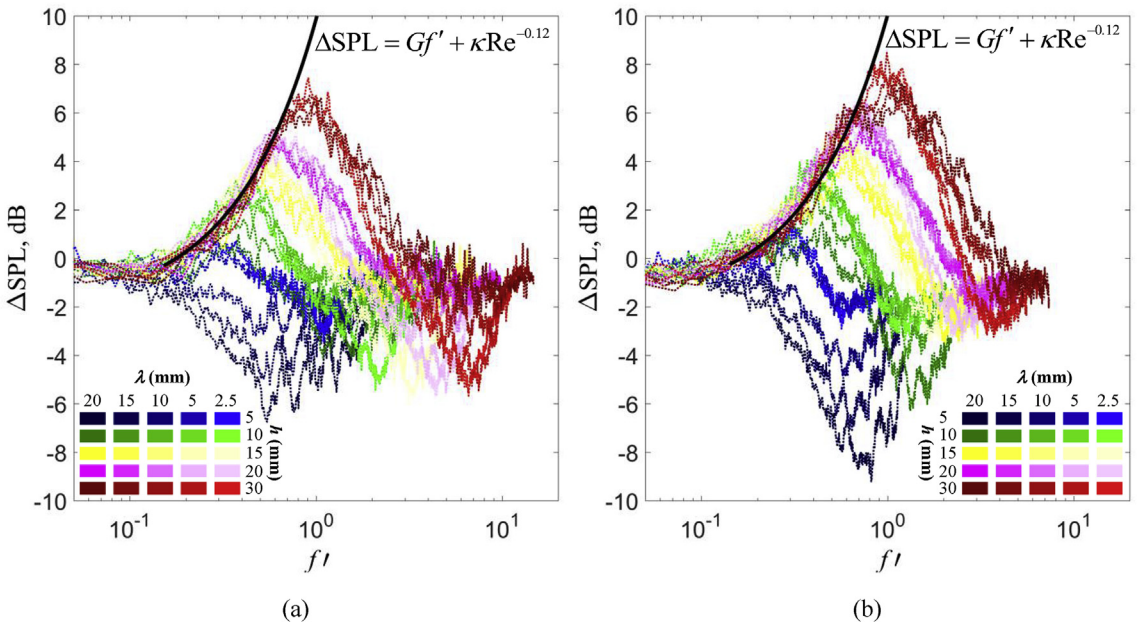

Fig. 6. ΔSPL (dB) spectra produced by the serrated leading edges of different λ and h at (a) $Re = 3 \times 10^5$ ($U_\infty = 30$ ms^{-1}), and (b) $Re = 6 \times 10^5$ ($U_\infty = 60$ ms^{-1}). Note that $f' = fh/U_\infty\,(\lambda/C)^{0.2}$.

dominant than the serration wavelength, λ, in the broadband noise reduction. The subsequent roll-off of the ΔSPL following the peaks simply means that the leading edge noise is becoming less dominant at higher frequencies, and as a result, the serrated leading edge devices also become less effective in reducing the noise level as manifested by the continual drop in the ΔSPL. It is also observed that an increase in noise, i.e. ΔSPL < 0, was found for the majority of the serrated leading edges tested here. The general trend observed for $f' > 1$ is that the starting frequency for noise increase tends to become higher as h increases.

It is interesting to examine the characteristics of the ΔSPL achieved by the 25 serrated leading edge cases with different combinations of λ and h as a function of f' and Re. This is shown in Fig. 7 by the ΔSPL contour maps. It is apparent that the combination of the two governing geometrical parameters λ and h can yield very different noise reduction capabilities for the straight-serrated aerofoil. It was found that the highest ΔSPL is usually associated with small λ and large h.

Two extreme serration cases are compared here: the $\lambda 2.5h30$ versus $\lambda 20h5$. Serration $\lambda 2.5h30$ can achieve the largest level of noise reduction at ΔSPL = 7–8 dB. For $2 \times 10^5 \leq Re \leq 6 \times 10^5$, the non-dimensional frequency range over which +ΔSPL can be achieved is $0.2 \leq f' \leq 2.5$. The mechanism underpinning the broadband noise reductions by $\lambda 2.5h30$ is conjectured to be associated with the serrations acting as a physical 'filter' and break-up device for the incoming turbulent flow structure. This point is illustrated in the schematic in Fig. 8, which shows that as the incoming turbulent flow structures impinge the sawtooth edge of $\lambda 2.5h30$, eddies of length scale greater than λ can be broken-up. For small λ, the sharp serration angle will force the turbulent eddies to 'stretch' and break-up further as they propagate downstream. Therefore, by the time the smaller-scale turbulent eddies reach the troughs, the lower level of turbulence intensity is manifested into a lower level of broadband noise radiation in the noise spectra presented here.

The other extreme serration case is the $\lambda 20h5$ serrated leading edge, where a significant noise increase between −5 and −10 dB for $f' > 0.4$ has been demonstrated. The level of noise increase is found to be more significant at higher Re. For example,

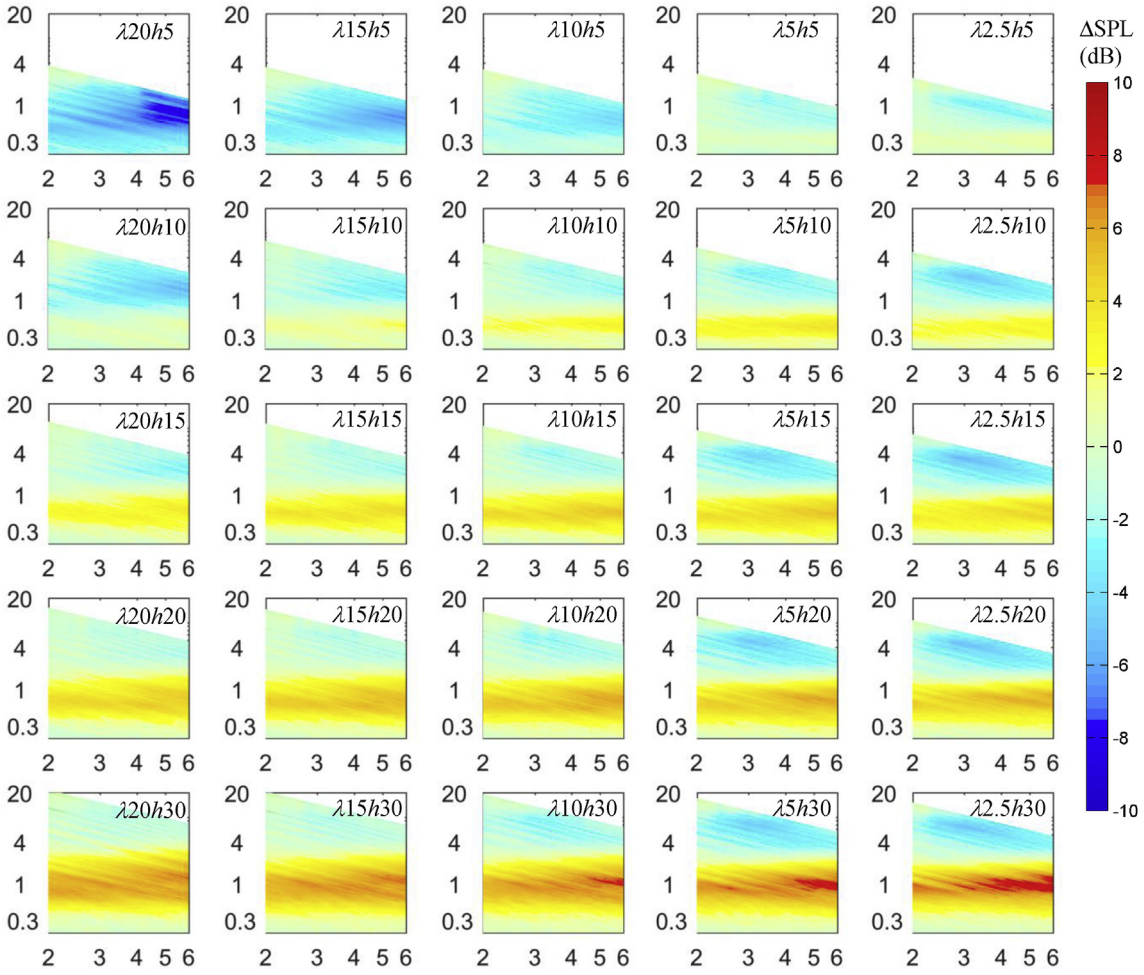

Fig. 7. Contour maps of the ΔSPL (dB) produced by different combinations of λ and h for the serrated leading edges. The abscissa is the Re ($\times 10^5$), and the ordinate is the f'.

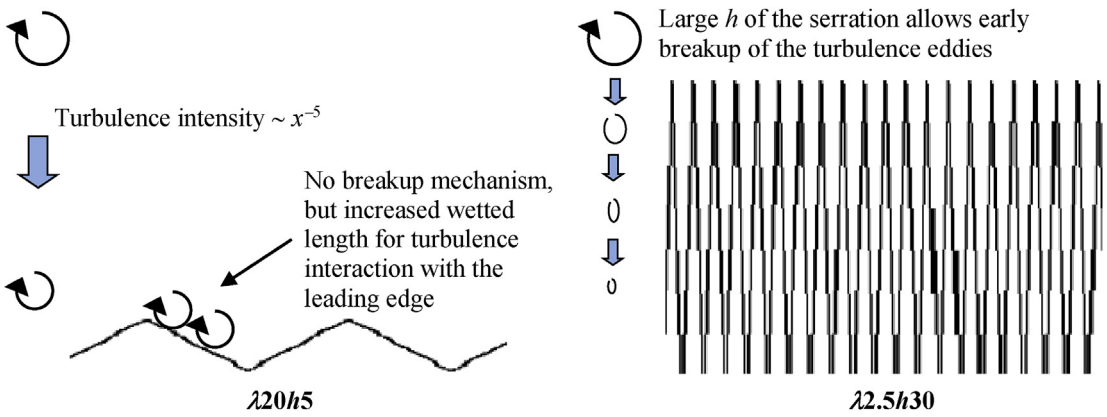

Fig. 8. Schematics illustrating the interactions between the turbulence structure and the different serration sawtooth geometries ($\lambda 20h5$ and $\lambda 2.5h30$), and their implication to the noise reduction/increase.

the ΔSPL for $Re > 4.5 \times 10^5$ is between −9 and −10 dB. Referring to the schematic in Fig. 8, the significant noise increase observed in the $\lambda 20h5$ case could also be related to the different responses of the turbulence structures to the specific serration geometry. Assuming the same turbulence structures as the $\lambda 2.5h30$ case, but this time convected towards the $\lambda 20h5$ serrated leading edge, the only dissipation mechanism [14] of such grid-generated structures would be a natural decay proportional to streamwise distance to the power of −5. The turbulence structures encountering the $\lambda 20h5$ serrated leading edge will not experience the same kind of forced breaking-up as in the $\lambda 2.5h30$ case. As a result, the intensity of the freestream turbulence can be better preserved at the vicinity of the serrated edges. The increased wetted length of the $\lambda 20h5$ serration (as a result of the large serration angle and short serration amplitude) also provides an enhanced interaction with the turbulence structures compared to the baseline $\lambda 0h0$. As a result, the ΔSPL becomes predominantly negative as manifested in the noise spectra.

It is also found that serrated leading edge devices with low λ (e.g. $\lambda 2.5h5$, $\lambda 2.5h10$, $\lambda 2.5h15$, $\lambda 2.5h20$ and $\lambda 2.5h30$) always trigger noise increase at high frequency. The level of noise increase is also found to be a function of h. The underlying mechanism could be related to their greater number of serration sawteeth per unit span, which will enhance the fluid-structural interaction noise between the turbulence eddies and the sawtooth oblique edges. When the h of the serrations is increased but with a fixed λ, the serration angle ϕ (see the definition in Section 2.2) reduces which makes the sawtooth edges less orthogonal to the flow direction. Therefore, the incoming turbulent flow is forced to pass through many narrow passages, thereby generating high frequency interaction noise in the process.

The serrated leading edge $\lambda 20h30$ has an outstanding noise reduction performance as it has been shown to provide +ΔSPL within a frequency range of $0.2 \leq f' \leq 4.5$, which is wider than that of $\lambda 2.5h30$, between $Re = 2 \times 10^5$ and 6×10^5. On average, the $\lambda 20h30$ serrated leading edge can achieve a ΔSPL between 4 and 7 dB. Furthermore, the $\lambda 20h30$ serration design does not result in a noise increase at higher frequencies, which is a common feature for the serrated leading edge with low λ as discussed in the previous paragraph. When $\lambda 20h30$ is compared with $\lambda 2.5h30$ (both have the same h but with different λ), two features can be observed:

1. Although $\lambda 2.5h30$ has the largest absolute ΔSPL level, the $\lambda 20h30$ actually possesses a much larger frequency range ($\Delta f' = 4.4$) where noise reduction +ΔSPL is achieved.
2. Although both have the same h, compared to the $\lambda 2.5h30$ case, $\lambda 20h30$ has a larger serration angle ϕ and a reduced total number of sawtooth serrations per unit span. As a result, the generation of the turbulence-structure interaction noise at high frequency is less significant for $\lambda 20h30$.

It is generally observed that the level of noise reduction is the most sensitive to the serration amplitude h. To examine the overall effect, the overall sound pressure level OASPL is calculated for all serrated leading edge cases, including the baseline $\lambda 0h0$. The OASPL is obtained by integrating the mean-square acoustic pressure from 50 Hz to 20 kHz. Here the level of OASPL reduction is represented by ΔOASPL, which is defined as $\text{OASPL}(\lambda 0h0) - \text{OASPL}(\lambda x h y)$, where $x \in 2.5, 5, 10, 15, 20$ mm, and $y \in 5, 10, 15, 20, 30$ mm. Fig. 9 shows the various ΔOASPL achieved by all the serrated leading edges. Similarly, a positive ΔOASPL denotes noise reduction, and a negative one denotes noise increase.

It can be seen that the sensitivity of the noise performance to h gradually decreases when λ is reduced. The ΔOASPL plots provide a good indication on the overall performance of the serrations. It can be seen that, although the serration $\lambda 2.5h30$ has produced the largest level of noise reduction in terms of SPL, it can only achieve a maximum ΔOASPL of about 1.5 dB at $Re = 2 \times 10^5$. This is because the OASPL in this case also includes the contribution of noise increases at high frequency. As a result, the overall noise performance of this particular serration design is not satisfactory. Another serration $\lambda 20h30$, however,

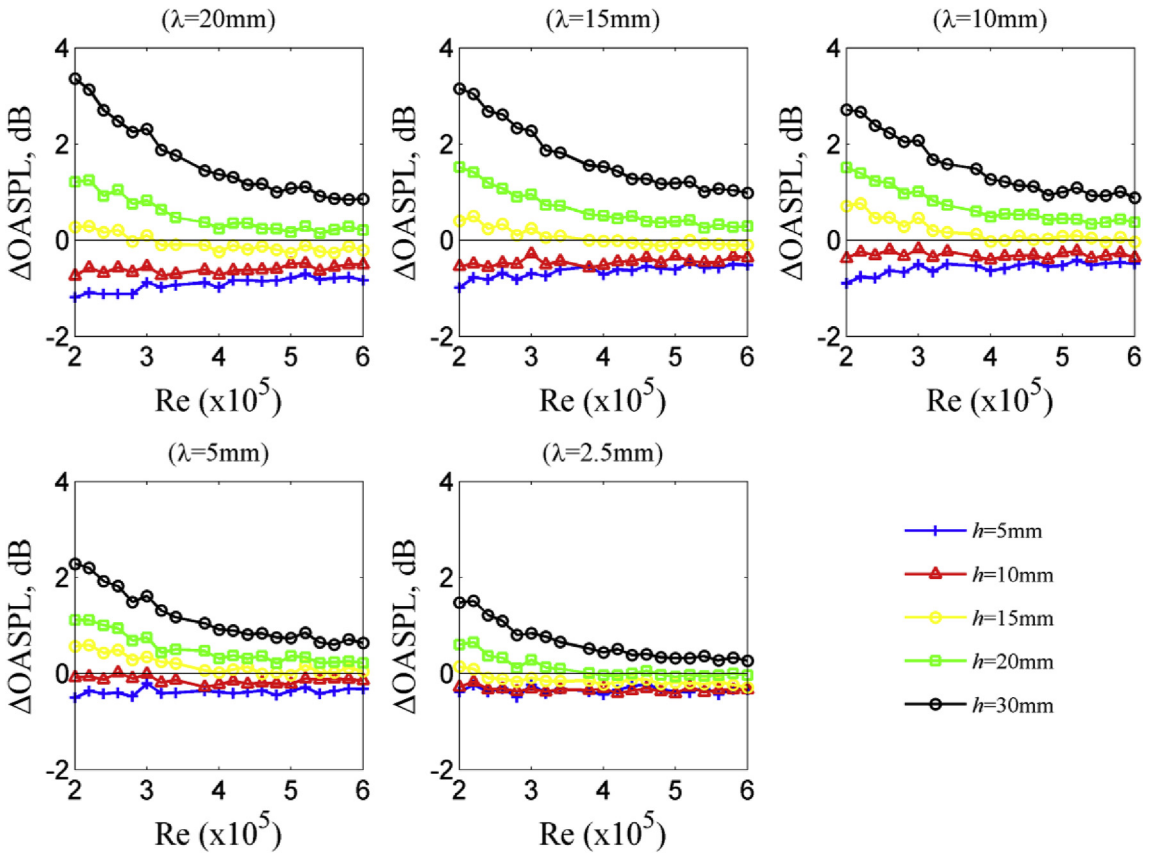

Fig. 9. ΔOASPL (dB) produced by the serrated leading edges of different λ and h at $Re = 2–6 \times 10^5$ ($U_\infty = 20–60\,\mathrm{ms}^{-1}$).

can achieve an improved ΔOASPL of about 3.4 dB at the same *Re*. This is due to the fact that high frequency noise increase is absence for this particular serration design. The ΔOASPL results also highlight another observation in terms of the noise reduction capability. It can be seen that the serrations tend to undergo a decrease in performance with increasing U_∞ or *Re*. The serration $\lambda 20h30$ is found to achieve the best performance, with ΔOASPL decreasing from 3.4 dB at $Re = 2 \times 10^5$ to 0.9 dB at $Re = 6 \times 10^5$. For serrations with identical h, the sensitivity of ΔOASPL with respect to *Re* increases for large λ.

It has been shown that the most optimised leading edge serration that achieves a very large reduction in broadband noise level at low frequencies, yet does not produce any noise increase at high frequencies, is the $\lambda 20h30$ type. This particular serration is therefore selected for the study into the effect of geometrical angles of attack α on noise reduction. Note that the geometrical angle of attack α does not represent the true angle of attack due to the open jet deflection. Noise measurements were taken with the aerofoil placed in the freestream flow at $0^\circ \le \alpha \le 10^\circ$ across $2 \times 10^5 \le Re \le 4 \times 10^5$. The reason for not investigating higher *Re* is to avoid possible fluttering of the serrated flat plate devices at large α.

Fig. 10a and b shows the SPL spectra produced by $\lambda 0h0$ and $\lambda 20h30$, respectively, at $0 \le \alpha \le 10^\circ$ and $Re = 3 \times 10^5$. It can be seen that for the baseline $\lambda 0h0$, the SPL spectra are not very sensitive to the change in α. By contrast, the SPL produced by the $\lambda 20h30$ serrated leading edge increases with α up to 3 dB (against the level at $\alpha = 0^\circ$) for 600 Hz < f < 1.6 kHz; and up to 12 dB for $f \ge 1.6$ kHz. Contour maps of ΔSPL comparing $\lambda 0h0$ to $\lambda 20h30$, as a function of U_∞ and f, are shown in Fig. 10c for various α. Only minor changes in ΔSPL are observed from $\alpha = 0^\circ$ to 2° due to the relatively small change in the 'effective' angle of attack. At $\alpha = 4^\circ$, the level of broadband noise reduction and the corresponding frequency range (Δf) start to reduce. At the same time, the increase of the high frequency noise becomes more prominent. This trend continues as α increases. Between $\alpha = 8^\circ$ and 10°, the level of the broadband noise reduction has become very low, whilst significant noise increase can be found at the high frequency region. Overall, the serration becomes less effective as the angle of attack is increased.

4. General aeroacoustic characteristics of the curved-serrated leading edges

As stated in Section 1, another objective of this paper is to investigate whether implementing a curved-serration on the leading edge could further improve the broadband noise reduction. The hypothesis is based on the geometrical consideration that the curved-flow path within the sawtooth gap/passage will yield a more effective serration amplitude h', which is normally larger than the h counterpart for an otherwise straight-serration. As already discussed extensively in the previous

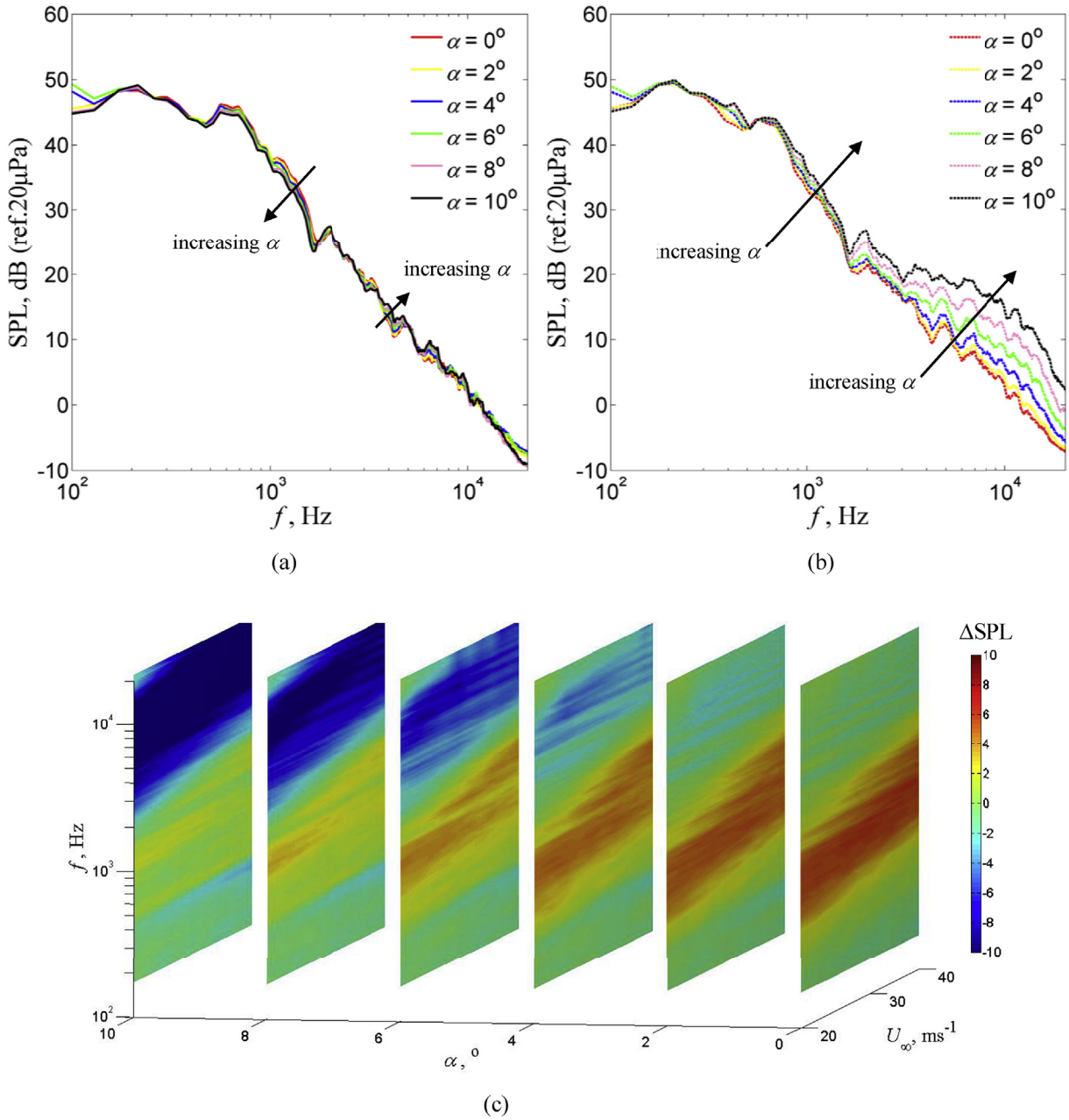

Fig. 10. SPL spectra (dB, ref 20 μPa) measured at $\alpha = 0°–10°$ and $Re = 3 \times 10^5$ ($U_\infty = 30\ \mathrm{ms}^{-1}$) for (a) unmodified baseline leading edge $\lambda 0h0$, and (b) $\lambda 20h30$ serrated leading edge. (c) Sensitivity of the ΔSPL (dB) to the α. Contour maps are presented as a function of U_∞ and f.

section, large serration amplitude is more effective to achieve a higher level of positive ΔSPL. As a reminder, three additional geometric parameters are used to describe a curved-serration. These are the inclination angle i, the curvature R and the effective serration amplitude h' (see Fig. 3b). Similarly, the experiments for the curved-serration cover $2 \times 10^5 \leq Re \leq 6 \times 10^5$, while α was fixed at $\alpha = 0°$.

It should be mentioned that the curve-serration will only make sense when h is sufficiently large. Therefore, this paper only examines the results of the curved-serrated leading edges at $h = 30$ mm. Fig. 11a shows the SPL spectra for the large serration wavelength $\lambda = 20$ mm, which include $\lambda 20h30$(straight), $\lambda 20h30(i15°R50)$, $\lambda 20h30(i15°R100)$, $\lambda 20h30(i30°R50)$ and $\lambda 20h30(i30°R100)$ at $Re = 6 \times 10^5$. The SPL spectrum produced by the baseline $\lambda 0h0$ is also included in the figure for comparison. Note that, unless stated otherwise, any reference of "noise reduction" or "noise increase" in the subsequent discussion is measured against the $\lambda 0h0$ baseline case. The straight-serration $\lambda 20h30$(straight) is shown to achieve noise reduction for $f > 850$ Hz. As can be seen in Fig. 11a, the curved-serrated leading edge cases are incapable of matching the level

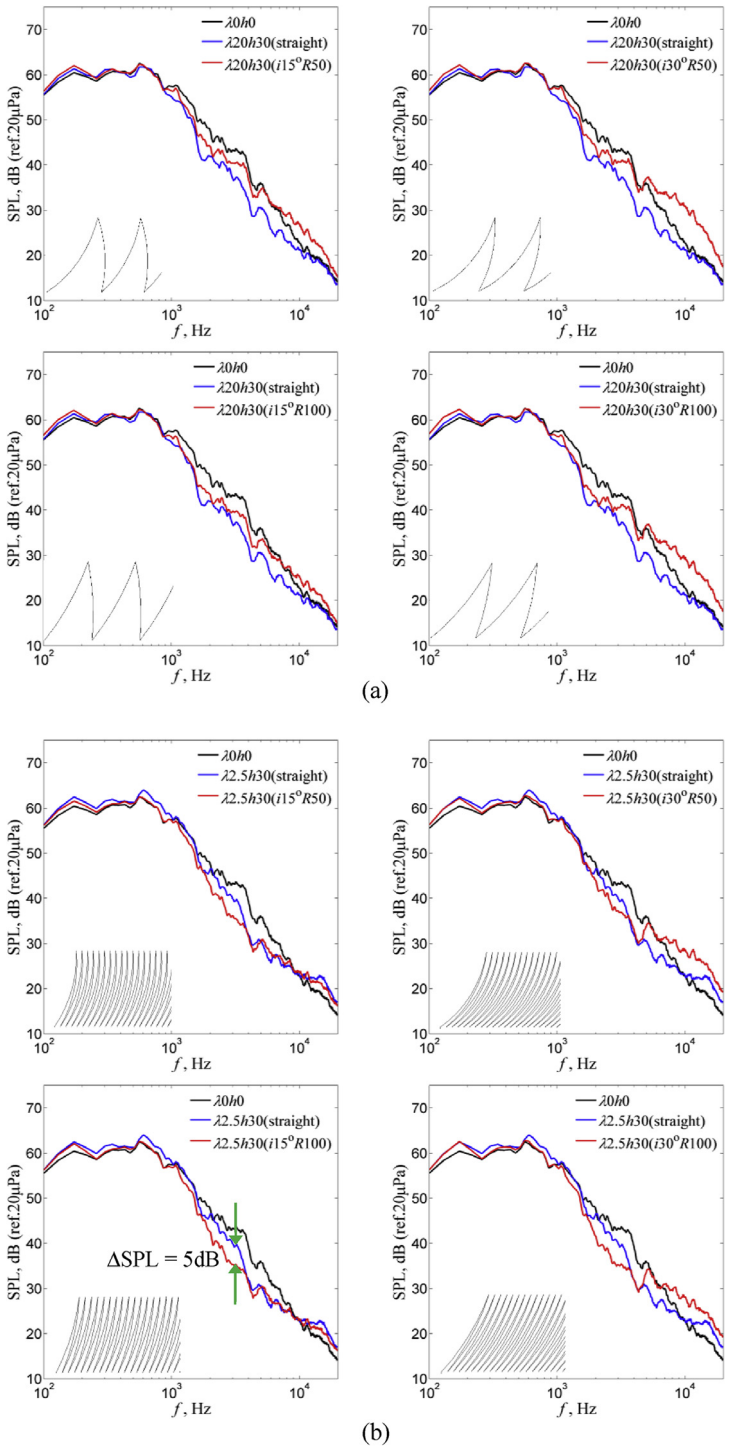

Fig. 11. Comparisons of the SPL (dB, ref 20 μPa) spectra between the straight and curved serrated leading edges for the cases of (a) $\lambda 20h30$, and (b) $\lambda 2.5h30$, at $Re = 6 \times 10^5$ ($U_\infty = 60\ \mathrm{ms}^{-1}$).

of noise reduction achieved in the $\lambda 20h30$(straight) case. For cases with a large inclination angle ($i = 30^\circ$), such as $\lambda 20h30(i30^\circ R50)$ and $\lambda 20h30(i30^\circ R100)$, a significant noise increase is even observed for $f > 4.8$ kHz.

However, as shown in Fig. 11b, more encouraging results can be obtained when the curved-serration has a smaller serration wavelength, i.e. $\lambda = 2.5$ mm. With a smaller inclination angle ($i = 15^\circ$), both $\lambda 2.5h30(i15^\circ R50)$ and $\lambda 2.5h30(i15^\circ R100)$

could achieve an even lower broadband noise radiation (5 dB lower at the same frequency) than the $\lambda 2.5h30$(straight) serration within the frequency range of $1 < f < 3.8$ kHz. Previously, noise increase has been observed for the $\lambda 2.5h30$(straight) at high frequency (see Figs. 6 and 7). This also happens for the $\lambda 2.5h30(i15^\circ R50)$ and $\lambda 2.5h30(i15^\circ R100)$ curved-serrations, but the level of noise increase is less. When a large inclination angle is used ($i = 30^\circ$), such as the $\lambda 2.5h30(i30^\circ R50)$ and $\lambda 2.5h30(i30^\circ R100)$ curved-serrations, they still outperform the straight-serration counterpart for $1 < f < 3.8$ kHz. However, for $f > 5$ kHz, these curved-serrated leading edges with a larger inclination angle undergo a jump in the SPL to significantly surpass the noise level produced by the baseline $\lambda 0h0$. This phenomenon is very similar to the one observed in the cases with large serration wavelength, but identical inclination angle. i.e. $\lambda 20h30(i30^\circ R50)$ and $\lambda 20h30(i30^\circ R100)$, presented earlier in Fig. 11a.

So far, it is clear that a sufficiently large inclination angle i (e.g. $i = 30^\circ$) is prone to produce a significant noise increase at high frequency. The level of noise increase is even higher than those produced by the baseline $\lambda 0h0$ and the corresponding straight-serrations. A curved-serrated leading edge with large inclination angle will result in a more inclined and outward tip (compare the insert drawings of Fig. 11). For both the straight-serrated and curved-serrated leading edges with small inclination angle, flow leaving their tips will predominantly develop into wall-bounded flow (e.g. the boundary layer) at downstream. However, the flow leaving a sufficiently inclined-tip will be more similar to a turbulent free shear flow. Assuming that the scale of the turbulent eddies generated by these tips is rather small, the interaction of the free shear flow with the downstream leading edge would result in an elevated level of noise radiation at high frequency.

Based on the results in Fig. 11, the introduction of curved-serration to the leading edge can generate the following two main outcomes: (1) outperform the straight-serration in terms of the broadband noise reduction at the mid-frequency region, provided that the serration wavelength λ is relatively small, and (2) achieve a reduced level of noise increase at high frequency when the inclination angle i is small.

The two outcomes mentioned above were derived from Fig. 11 where $Re = 6 \times 10^5$. They are also valid when subjected to different Reynolds numbers. These are demonstrated in Fig. 12a–b by the contour maps of ΔSPL as a function of Re and f between the baseline $\lambda 0h0$, and either the straight-serration or the curved-serration. When the curved-serrated leading edge is subjected to the optimal configuration, for example the $\lambda 2.5h30(i15^\circ R100)$ case, it can convincingly outperform the $\lambda 2.5h30$(straight) counterpart. To illustrate this in a quantifiable way, Fig. 12c shows the ΔSPL′ as a function of Re and f between the $\lambda 2.5h30$(straight) and the $\lambda 2.5h30(i15^\circ R100)$. A positive level denotes that the curved-serration would produce a lower noise level than that by the straight-serration. It is clear from the figure that a further broadband noise reduction of ΔSPL′ = 5 dB can be achieved by the curved-serration at the mid-frequency region across the entire Reynolds number range. Moreover, noise level at the high-frequency region radiated by the curved-serration is also lower than that by the straight-serration, as demonstrated by the positive level of ΔSPL′.

The analysis thus far of the acoustic spectra pertaining to the curved-serration only focuses on the dimensional frequency. The next step is to establish whether the ΔSPL produced by the curved-serration can follow the scaling law in Eq. (1), which was originally derived from the straight-serration results. For the curved-serrations, one of the length scales used in the non-dimensional frequency f', i.e. the serration amplitude, is now substituted by the h'. Note that h' for the serration inclination angles $i = 15^\circ$ and 30° is approximately 32 and 36 mm, respectively. The level of serration curvature radius R will not affect h' very significantly. Fig. 13 shows the ΔSPL against f' for the $\lambda 2.5h30$(straight), and several curved-serration variants $i15^\circ R50$, $i15^\circ R100$, $i30^\circ R50$ and $i30^\circ R100$, at two different Reynolds numbers. As expected, the ΔSPL spectra, pertaining to the straight-serration, are well-bounded by the limiting-line at $f' < 1$ when the original gradient $G = 12$ is used in Eq. (1). However, a better fit for most of the curved-serrations against the limiting-line, with the exception of the $i30^\circ R50$ case, is established with a gradient of $G = 14$. The best fit for the curved-serrations is also confined to $0.5 \leq f' \leq 1$.

The results in Fig. 13 thus provide several indications about the possible mechanisms underpinning the further broadband noise reduction by the curved-serration. First, the fact that the same frequency scaling as per Eq. (1) can still be applied to the curved-serrated leading edges would indicate that one of the mechanisms must be associated with the increase of the "effective" serration amplitude h' although its "normal" serration amplitude h actually remains the same as in the straight-serration counterpart ($\lambda 2.5h30$). Second, the increase of the gradient G from 12 to 14 for the limiting-line at $0.5 \leq f' \leq 1$ demonstrates a significant improvement of the noise reduction capability that is otherwise not achievable by a standard straight-serrated leading edge for any combinations of λ and h. The reason for such improvement by the curved-serration in the interaction noise reduction can be investigated from a hydrodynamic point of view in the future studies.

For both the straight and curved-serrated leading edges, it has been observed that the maximum level of noise reduction, i.e. $\Delta SPL_{(max)}$, can be captured by the limiting-lines depicted in Fig. 13. Fig. 14 shows the contour maps of $\Delta SPL_{(max)}$, as a function of h or h' and Re, for two serration curvature radii, $R = 50$ and 100 mm. Note that $h' > 30$ mm corresponds to the curved-serrated leading edge. Below which, the serration is of the straight type and the amplitude is represented by h. Not surprisingly, at $h \leq 30$ mm the level of $\Delta SPL_{(max)}$ is found to increase with h. More interestingly, for a fixed h, the level of $\Delta SPL_{(max)}$ increases with Re. This suggests that, for a particular serrated leading edge, the highest absolute level of noise reduction usually occurs at high Re.

For the $R = 50$ mm case of the curved-serration, there is an increase of $\Delta SPL_{(max)}$ from 7 to 8 dB for $30 < h' \leq 32$ mm in the high Re region. This is contrasted by a slight drop of $\Delta SPL_{(max)}$ from 7 to 6 dB at $32 \leq h' \leq 36$ mm in the low Re region, although further study is needed to determine the cause of this drop. A much improved performance can be obtained when the

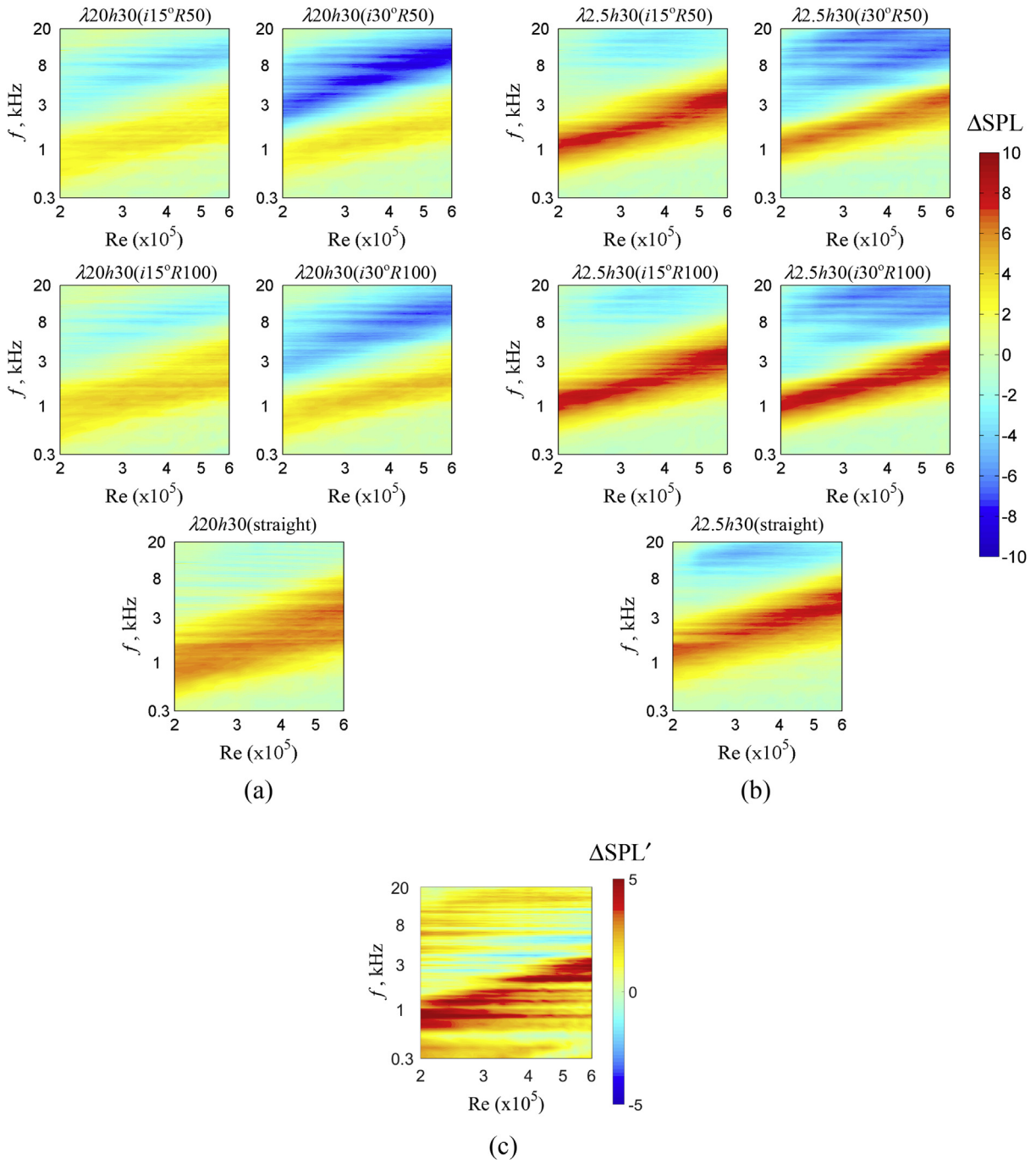

Fig. 12. (a, b) Sensitivities of the ΔSPL (dB) to the inclination angle (i) and curvature radius (R) for the serrated leading edges $\lambda 20h30$ and $\lambda 2.5h30$, respectively; (c) ΔSPL′ (dB) between $\lambda 2.5h30$(straight) and $\lambda 2.5h30(i15^{\circ}R100)$.

serration curvature radius is increased to $R = 100$ mm, where the region of $32 \leq h' \leq 36$ mm across the entire Re shows a noise reduction between $\Delta SPL_{(max)} = 8$ and 9 dB.

5. Aerodynamic forces produced by the straight- and curved-serrated leading edges

For a thin aerofoil subjected to an elevated freestream turbulence level, the sensitivities of the radiated noise level by the add-on type serrated leading edges to the serration geometries (amplitude, wavelength, and for the curved-serration: the

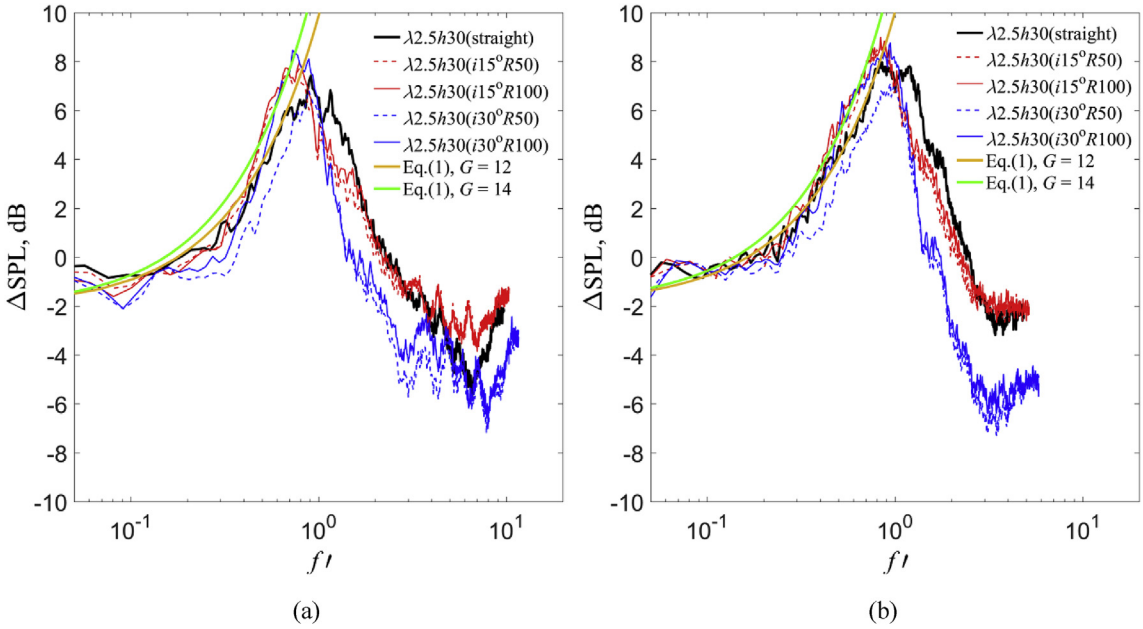

Fig. 13. Comparison of ΔSPL (dB) spectra produced by the straight and curved-serrated leading edges at (a) $Re = 3 \times 10^5$ ($U_\infty = 30\,\mathrm{ms}^{-1}$), and (b) $Re = 6 \times 10^5$ ($U_\infty = 60\,\mathrm{ms}^{-1}$). Note that $f' = fh/U_\infty\,(\lambda/C)^{0.2}$ for the straight-serration, and $f' = fh'/U_\infty\,(\lambda/C)^{0.2}$ for the curved-serration.

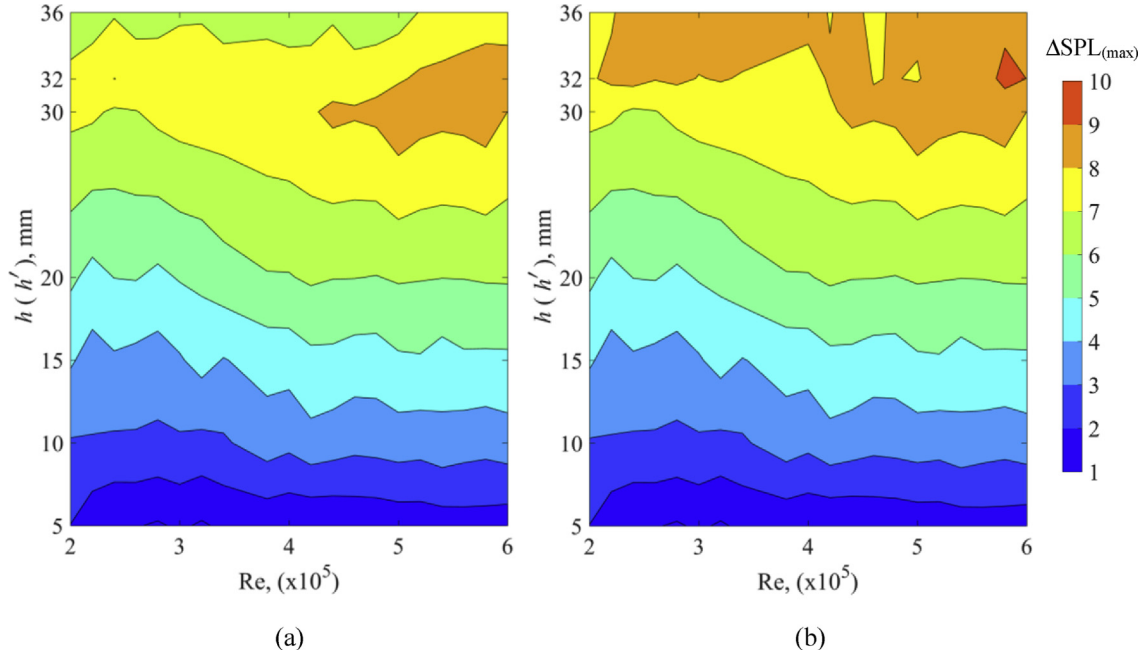

Fig. 14. $\Delta SPL_{(max)}$ (dB) as a function of serration amplitude h (h') and Reynolds number Re for the λ2.5h30 serrated leading edge. For the curved-serration ($h' > 30$ mm), comparison is made between the curvature radius of (a) $R = 50$ mm, and (b) $R = 100$ mm.

inclination angle and curvature radius), Reynolds number and geometrical angle of attack have been discussed in Sections 3 and 4. Although some of them have demonstrated excellent broadband noise reduction capabilities, the question still remains whether gains in the aeroacoustic performance by the serrated leading edges could be offset by aerodynamic penalties, if any. Although not exhaustive, this paper seeks to address this question by conducting direct aerodynamic force measurements for some of the serrated leading edges studied previously. The experiments were conducted in a separate wind tunnel with a

closed-test section (0.5 m × 0.5 m cross-section), which is now referred to as the "aerodynamic wind tunnel". It should be stated that the flow conditions generated in the aerodynamic wind tunnel will be different from the open-jet aeroacoustic wind tunnel in terms of the freestream turbulence intensities (0.3% vs. 3.7% for the aerodynamic and aeroacoustic experiments, respectively). Due to the global jet deflection, the "geometrical" angle of attack α for the NACA0008 aerofoil in a finite open-jet wind tunnel will not be equal to the "effective" angle of attack $\alpha_{(\text{effective})}$. It is unrealistic to achieve a large $\alpha_{(\text{effective})}$ from the open-jet wind tunnel which is mainly used for the aeroacoustic test. To measure the aerodynamic forces at large $\alpha_{(\text{effective})}$, the aerodynamic wind tunnel was used instead.

Several non-dimensional aerodynamic terms are of interest in the analysis. These are the lift coefficient C_L, the drag coefficient C_D, and the lift-to-drag ratio C_L/C_D. Note that $C_L = 2L/\rho U_\infty^2 S$ and $C_D = 2D/\rho U_\infty^2 S$, where ρ is the air density, S is the planform area of the aerofoil, L and D are the lift and drag forces measured directly from the force balance, respectively. The aerodynamic forces for each leading edge devices (baseline, straight- or curved-serration) were measured from $\alpha_{(\text{effective})} = 0^\circ$ to 20° with an incremental step of 1°. The freestream velocity U_∞ is maintained at 24 ms^{-1}, corresponding to a Reynolds number of about 2.4×10^5, throughout the experiment. The ΔC_L, ΔC_D and $\Delta(C_L/C_D)$ can be defined as:

$$\Delta C_L = C_{L\ (\text{serrated})} - C_{L\ (\lambda 0 h 0)}$$

$$\Delta C_D = C_{D\ (\text{serrated})} - C_{D\ (\lambda 0 h 0)}$$

$$\Delta(C_L/C_D) = (C_L/C_D)_{(\text{serrated})} - (C_L/C_D)_{(\lambda 0 h 0)} \tag{2}$$

Positive and negative values of ΔC_L represent gains and losses in the lift coefficient, respectively, when a serrated leading edge is used. Positive and negative values of ΔC_D represent increases and decreases in the drag coefficient, respectively, by the serrated leading edge. Finally, positive and negative values of $\Delta(C_L/C_D)$ represent gains and losses in the lift-to-drag ratio, respectively, by the serrated leading edge.

Fig. 15 shows the C_L, C_D, and C_L/C_D over $0^\circ \le \alpha_{(\text{effective})} \le 20^\circ$ for the baseline ($\lambda 0 h 0$), and several types of straight- and curved-serrated leading edges that have previously been demonstrated as superior in the reduction of the interaction broadband noise. In Fig. 15a, the $\lambda 0 h 0$ baseline leading edge follows the thin aerofoil theory quite well where the lift curve slope, $dC_L/d\alpha_{(\text{effective})} \approx 0.1$ between $0 < \alpha_{(\text{effective})} \le 9^\circ$ (pre-stall flow regime). Between $9^\circ < \alpha_{(\text{effective})} \le 12^\circ$ (transitory flow regime), the C_L "plateaus" at around 0.8. The stall angle is found to occur at $\alpha_{(\text{effective})} \approx 12^\circ$. At $\alpha_{(\text{effective})} > 12^\circ$ (post-stall flow regime), the C_L begins to drop, albeit not too abruptly. For analysis purpose, the following discussions will take reference to the three flow regimes (pre-stall, transitory and post-stall) as defined by the variation of C_L against the $\alpha_{(\text{effective})}$ for the $\lambda 0 h 0$ baseline leading edge.

The levels of C_L and lift curve slopes, $dC_L/d\alpha_{(\text{effective})}$, for the $\lambda 20 h 30$ and $\lambda 20 h 30(i15^\circ R100)$ serrated leading edges at the pre-stall flow regime are the same as the $\lambda 0 h 0$ baseline leading edge. In the transitory flow regime, although the serrated leading edges achieve a slightly lower level of C_L ($\Delta C_L \approx -0.06$) when compared to the $\lambda 0 h 0$ case, they still can maintain a positive $dC_L/d\alpha_{(\text{effective})}$. However, whilst the $dC_L/d\alpha_{(\text{effective})}$ for the $\lambda 0 h 0$ baseline understandably becomes negative at the post-stall regime, both serrated leading edge cases continues to exhibit positive $dC_L/d\alpha_{(\text{effective})}$ at a tenth of the pre-stall level, eventually achieving positive ΔC_L (i.e. better performance than the baseline leading edge) at $\alpha_{(\text{effective})} \ge 13^\circ$. The largest ΔC_L (≈ 0.11) is found to occur at $\alpha_{(\text{effective})} = 18^\circ$. Although not shown here for brevity, the above results can be corroborated by the surface oil flow visualisation where the vortices generated from the serration troughs have been shown to suppress the otherwise fully separated flow on the aerofoil suction side. Overall, the differences in the C_L and $dC_L/d\alpha_{(\text{effective})}$ between the $\lambda 20 h 30$ and $\lambda 20 h 30(i15^\circ R100)$ are not too significantly, although a slightly higher degradation in the C_L level by the curved-serrated leading edge was observed in the transitory flow regime.

For the $\lambda 2.5 h 30$ and $\lambda 2.5 h 30(i15^\circ R100)$ serrated leading edges, a significant loss in C_L compared to the baseline $\lambda 0 h 0$ can be observed throughout the pre-stall and transitory flow regimes. The largest degradation occurs at $\alpha_{(\text{effective})} = 10^\circ$ where $\Delta C_L = -0.27$. The $dC_L/d\alpha_{(\text{effective})}$ for both the serrated leading edges, however, are able to remain positive throughout the whole range of $\alpha_{(\text{effective})}$. The crossover where $\Delta C_L > 0$ occurs at $\alpha_{(\text{effective})} = 17^\circ$–$18^\circ$, above which the serrated leading edges begin to outperform the baseline $\lambda 0 h 0$. The above results also demonstrate that the curved-serration $\lambda 2.5 h 30(i15^\circ R100)$ can produce a slightly larger level of ΔC_L than the straight counterpart $\lambda 2.5 h 30$ in the post-stall flow regime.

Although the $\lambda 20 h 30$ and $\lambda 20 h 30(i15^\circ R100)$ serrated leading edges perform reasonably well regarding both C_L and boundary layer stall suppression, as shown in Fig. 15b both produce a positive ΔC_D, i.e. a higher drag than the baseline $\lambda 0 h 0$, across (almost) the entire range of $\alpha_{(\text{effective})}$. The only exception is the curved-serrated $\lambda 20 h 30(i15^\circ R100)$ case where ΔC_D is negative for $10^\circ \le \alpha_{(\text{effective})} \le 14^\circ$. The $\lambda 2.5 h 30$ and $\lambda 2.5 h 30(i15^\circ R100)$ serrated leading edges also largely follow the same trend. However, the negative ΔC_D now occurs at a larger range of $9^\circ \le \alpha_{(\text{effective})} \le 15^\circ$–$16^\circ$ for both the straight and curved-serrated leading edges. Furthermore, the level of drag increase is not as significant as in the $\lambda 20 h 30$ and $\lambda 20 h 30(i15^\circ R100)$.

In summary, when the serration amplitude is sufficiently large (i.e. $h = 30$ mm or $h/C = 0.2$), an increased performance in C_L (by having a large serration wavelength λ) usually attracts an increase in C_D. An opposite trend applies in the reverse scenario. This relationship applies to both the straight and curved-serrated leading edges. Because of this anti-correlation between C_L and C_D, the lift-to-drag ratios (C_L/C_D) produced by the $\lambda 2.5 h 30$ and $\lambda 2.5 h 30(i15^\circ R100)$ serrated leading edges are largely similar to those of the $\lambda 20 h 30$ and $\lambda 20 h 30(i15^\circ R100)$ counterparts, as depicted in Fig. 15c. Note that, as a metric for

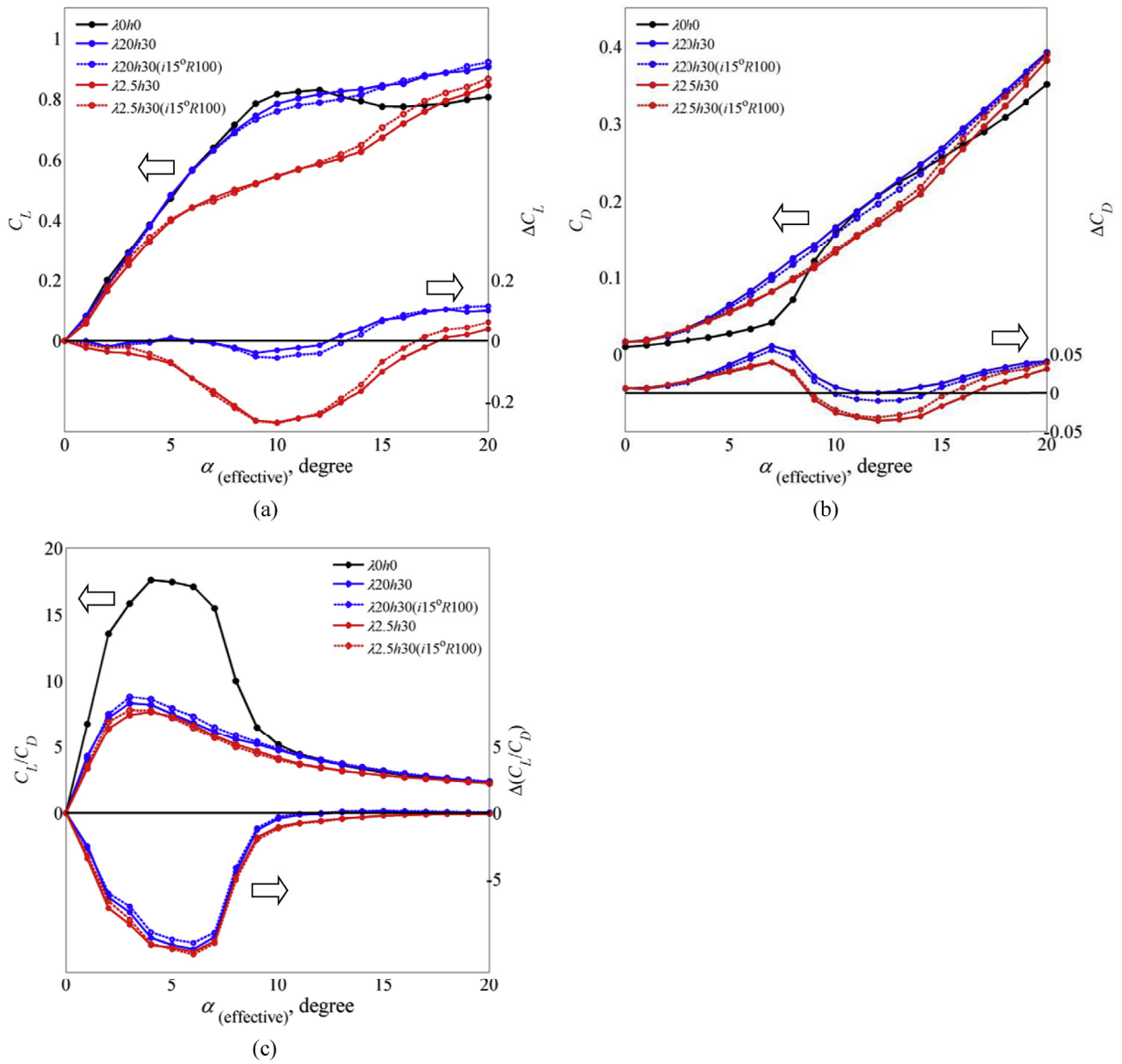

Fig. 15. Comparison of the (a) C_L & ΔC_L (b) C_D & ΔC_D and (c) C_L/C_D & $\Delta(C_L/C_D)$ for the baseline ($\lambda 0h0$) aerofoil and those subjected to straight- ($\lambda 20h30$ and $\lambda 2.5h30$) and curved-serrated ($\lambda 20h30(i15^\circ R100)$ and $\lambda 2.5h30(i15^\circ R100)$) leading edges at $Re = 2.4 \times 10^5$.

measuring the overall aerodynamic performance of an aerofoil, (C_L/C_D) should be as large as possible. The (C_L/C_D) produced by all the straight and curved-serrated leading edges are considerably lower than that the ratio produced by the baseline $\lambda 0h0$ case for the pre-stall flow regime. However, the difference between the baseline and the $\lambda 20h30$ family of serrated leading edges diminishes, i.e. $\Delta(C_L/C_D) \rightarrow 0$ at the transitory and post-stall flow regimes. To summarise the above behaviours, it is clear that both the straight and curved leading edge devices with large serration amplitude h and wavelength λ are effective in the post-stall regime in preventing boundary layer separation without scarifying the overall aerodynamic performance in terms of the lift-to-drag ratio.

It is also of interest to investigate the aerodynamic performance of the leading edge devices with small serration amplitude. Fig. 16a, b and 16c show the variations of C_L, C_D and (C_L/C_D) produced by the $\lambda 2.5h5$ and $\lambda 20h5$ leading edge devices across the same range of $\alpha_{(\text{effective})}$, respectively. The original values produced by the baseline $\lambda 0h0$ are also included for comparison. The $\lambda 2.5h5$ serrated leading edge is first analysed. Overall, it can be seen that $\lambda 2.5h5$ significantly outperforms its $\lambda 2.5h30$ counterpart in terms of (C_L/C_D) in the pre-stall, transitory and parts of post-stall flow regimes ($\alpha_{(\text{effective})} \leq 16^\circ$). Above this high angle of attack, both leading edge devices are on the same level as the baseline $\lambda 0h0$ leading edge. This particular advantage in the (C_L/C_D) achieved by the small serration amplitude leading edge device ($\lambda 2.5h5$) is attributed to its larger level

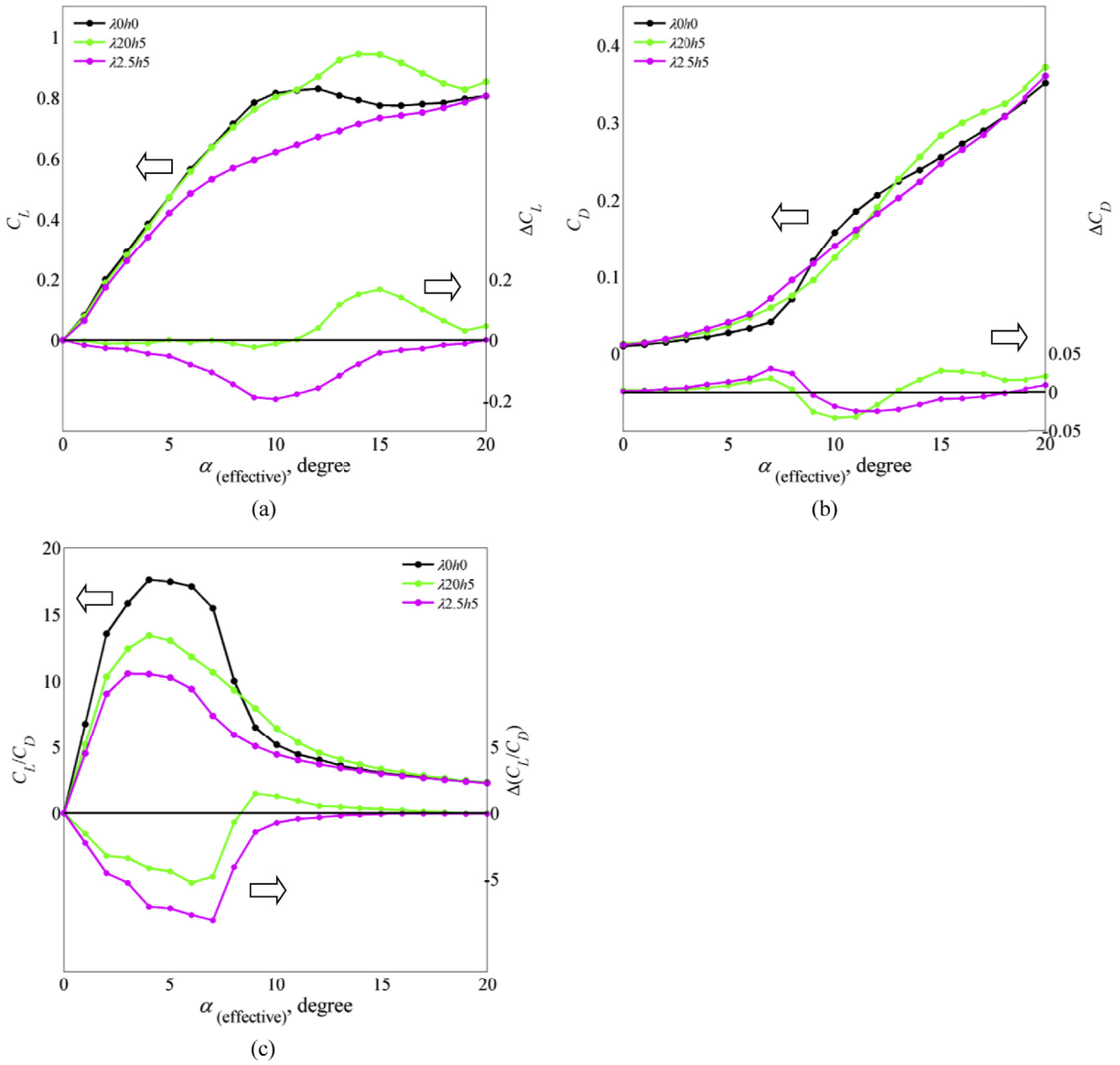

Fig. 16. Comparison of the (a) C_L & ΔC_L (b) C_D & ΔC_D and (c) C_L/C_D & $\Delta(C_L/C_D)$ for the baseline ($\lambda 0h0$) aerofoil and those subjected to straight-serrated leading edges ($\lambda 20h5$ and $\lambda 2.5h5$) at $Re = 2.4 \times 10^5$.

of C_L and lower level of C_D when compared to the $\lambda 2.5h30$ counterpart. The result suggests that a leading edge device with smaller serration amplitude could be more beneficial for the aerodynamic performance.

It is worth reminding that the results in Fig. 15a, indicating a good C_L performance, can be achieved by using a large serration wavelength for the leading edge device ($\lambda 20h30$). Indeed, this is further confirmed for the $\lambda 20h5$ case in Fig. 16. The C_L produced by the $\lambda 20h5$ serrated leading edge is at the same level as the baseline $\lambda 0h0$ across the entire pre-stall and transitory flow regimes. Moreover, the $\lambda 20h5$ serrated leading edge achieves a larger $C_{L(\max)}$ ($\Delta C_L = 0.2$) and stall angle (at $\alpha_{(\text{effective})} = 15^\circ$), simultaneously, than the baseline $\lambda 0h0$ leading edge without incurring as much drag penalty as its $\lambda 20h30$ counterpart. Also quite astonishingly, the C_D produced by the $\lambda 20h5$ serrated leading edge for $8^\circ \leq \alpha_{(\text{effective})} \leq 13^\circ$ is even lower than the baseline $\lambda 0h0$. As a consequence, the $\lambda 20h5$ serrated leading edge has improved its (C_L/C_D) performance across the entire range of $\alpha_{(\text{effective})}$, even surpassing the baseline $\lambda 0h0$ at $8^\circ \leq \alpha_{(\text{effective})} \leq 17^\circ$, i.e. the late pre-stall, entire transitory and most of the post-stall flow regimes.

6. Conclusion

This paper presents experimental results of the effect of add-on type leading edge serrations on the aeroacoustic and aerodynamic performances of a symmetrical NACA0008 aerofoil. For the aeroacoustic, the focus is on the turbulence-leading edge interaction broadband noise. Tests have been conducted in an aeroacoustic open jet wind tunnel at Brunel University London. 25 serrated leading edges (straight), that can be adequately described by their serration wavelength λ and serration amplitude h, have been investigated for Reynolds numbers, $0.2 \leq Re \leq 0.6$ millions. The sound pressure level reduction is found to be depend on h, λ and Re, and follows an empirical linear function of f' for a non-dimensional frequency $f' < 1$. Generally, it is found that serrations with large h are very effective in reducing the broadband noise levels up to about 8 dB ($\lambda 2.5h30$). However, the serration designs with smaller h can produce a noticeable increase in the level of noise at high frequency. The effect of λ on the noise reduction also depends on the corresponding h value. For example, the $\lambda 20h30$ case, which has the largest λ and h, has been shown to be a very effective configuration. However, the $\lambda 20h5$ case (same λ, but with the smallest h) can actually degrade the performance significantly with an increase in noise compared to the baseline aerofoil across the entire frequency range.

The curved-serration has been shown to be able to outperform its straight-serration counterpart by a further 5 dB broadband noise reduction when the right configuration (i.e. small serration wavelength λ, large serration amplitude h, small inclination angle i and large curvature radius R) is chosen. One of the main mechanisms is believed to be due to the increase of the "effective" serration amplitude h' as a result of the curvature although its "normal" serration amplitude h actually remains the same as the straight-serration counterpart. It is important to recognise that the curved-serration is able to increase the gradient G from 12 to 14 in Eq. (1), which demonstrates a significant improvement of the noise reduction capability that is otherwise not achievable by a straight-serrated leading edge for any combinations of λ and h. Currently, there is no evidence to fully support the hypothesis that the peak of the curved-serration can shield the grid-generated turbulence structures from reaching the serration troughs. Rather the results have shown that a curved-serration with a large inclination angle i, i.e. a more pronounced outward tip, can actually cause an increase of noise at high frequency, presumably due to the interaction between the tip-generated free shear turbulence and the downstream solid body.

To conclude, regarding the aerodynamic performance of the serrated leading edges, the most undesirable configuration is associated with a small λ and large h, i.e. $\lambda 2.5h30$. This configuration, however, has been shown earlier to be able to achieve the highest level of interaction noise reduction, ΔSPL. It is generally observed that the opposite combination of a large λ and a small h (e.g. $\lambda 20h5$), can be very effective in boundary layer stall suppression without incurring a large drag penalty, thereby recovering the overall aerodynamic performance in terms of the lift-to-drag ratio. Unfortunately, the very good aerodynamic performance of $\lambda 20h5$ under a non-elevated turbulence intensity of the freestream is associated with a poor aeroacoustic performance for the leading edge interaction noise when an elevated freestream turbulence intensity is present. Essentially, the $\lambda 20h5$ not only fails to achieve any interaction noise reduction across the entire Reynolds number and frequency ranges, but also radiates larger noise level than the baseline $\lambda 0h0$ leading edge.

The best compromise is found to be the $\lambda 20h30$ serrated leading edge. Aeroacoustically, this particular serrated leading edge device has been shown to produce a significant level of interaction noise reduction ΔSPL across the entire Reynolds number range, as well as across the widest range of frequencies amongst all the serrated leading edges. Furthermore, it does not produce an increase in noise at high frequencies. As a result, $\lambda 20h30$ has the highest level of reduction in the overall sound pressure level ΔOASPL. Aerodynamically, the $\lambda 20h30$ serrated leading edge surpasses the lift coefficient C_L of the baseline $\lambda 0h0$ leading edge for the entire post-stall flow regime (i.e. suppressing the boundary layer stall), and crucially, it maintains the same C_L in the pre-stall flow regime. The only downside is the relatively large level of drag coefficient C_D for most angles of attack, which results in a degradation of the overall aerodynamic performance in terms of the lift-to-drag ratio in the pre-stall and part of the transitory flow regimes. It is worth emphasising that the lift-to-drag ratio of the $\lambda 20h30$ and $\lambda 0h0$ leading edges for the post-stall flow regime remains largely identical.

Under a careful optimisation, the add-on type leading edge serration can be very effective in reducing turbulence-interaction broadband noise, as well as suppressing the boundary layer separation when subjected to a non-elevated free-stream turbulence. The nature-inspired concept of a curved-serration at the leading edge, which has been proven to be able to further enhance the reduction in broadband noise, provides an avenue for further development of other noise control techniques based on similar physical principles.

Acknowledgement

The authors would like to thank the financial supports from the EPSRC Doctoral Training Partnership (DTP), and the EPSRC Research Grant No: EP/N018737/1 on the "Quiet Aerofoils of the Next Generation".

References

[1] J.K. Staubs, Real Airfoil Effects on Leading Edge Noise, PhD thesis, Virginia Polytechnic Institute and State University, 2008.
[2] P. Soderman, Aerodynamic Effects of Leading Edge Serrations on a Two Dimensional Airfoil, NASA Technical Memorandum TM X-2643, 1972.
[3] A.S. Hersh, R.E. Hayden, Aerodynamic Sound Radiation from Lifting Surfaces with and without Leading-edge Serrations, NASA Contract Report No. 114370, 1971.

[4] V. Clair, C. Polacsek, T. Le Garrec, G. Reboul, M. Gruber, P.F. Joseph, Experimental and numerical investigation of turbulence-airfoil noise reduction using wavy edges, AIAA J. 51 (2013) 2695.
[5] S. Narayanan, P.F. Joseph, S. Haeri, J.W. Kim, P. Chaitanya, C. Polacsek, Noise Reduction Studies from the Leading Edge of Serrated Flat Plates, AIAA Paper No. 2014-2320, 2014.
[6] J.W. Kim, S. Haeri, P.F. Joseph, On the reduction of aerofoil-turbulence interaction noise associated with wavy leading edges, J. Fluid Mech. 792 (2016) 526.
[7] P. Chaitanya, P.F. Joseph, S. Narayanan, C. Vanderwel, J. Turner, J.W. Kim, B. Ganapathisubramani, Performance and mechanism of sinusoidal leading edge serrations for the reduction of aerofoil interaction noise, J. Fluid Mech. 818 (2017) 435.
[8] T.M. Biedermann, T.P. Chong, F. Kameier, C.O. Paschereit, Statistical-empirical modeling of airfoil noise subjected to leading edge serrations, AIAA J. 55 (2017) 3128.
[9] S. Ito, Aerodynamic influence of leading-edge serrations on an airfoil in a low Reynolds number, J. Biomech. Sci. Eng. 4 (2009) 117.
[10] A. Vathylakis, J.H. Kim, T.P. Chong, Design of a Low-noise Aeroacoustic Wind Tunnel Facility at Brunel University, AIAA Paper No. 2014-3288, 2014.
[11] T.P. Chong, A. Vathylakis, A. McEwen, F. Kemsley, C. Muhammad, S. Siddiqi, Aeroacoustic and Aerodynamic Performances of an Aerofoil Subjected to Sinusoidal Leading Edges, AIAA Paper No. 2015-2200, 2015.
[12] A. Pope, J. Barlow, W.J. Rae, Low-speed Wind Tunnel Testing, third ed., John Wiley and Sons, 1999.
[13] T. Bachmann, S. Klan, W. Baumgartner, M. Klaas, W. Schroder, H. Wagner, Morphometric characterisation of wing feathers of the barn owl *Tyto alba pratincola* and the pigeon Columba livia, Front. Zool. 4 (2007) 23.
[14] E.M. Laws, J.L. Livesey, Flow through screens, Annu. Rev. Fluid Mech. 10 (1978) 247.